© 2016. Published by The Company of Biologists Ltd | Journal of Cell Science (2016) 129, 4278-4288 doi:10.1242/jcs.194878

RESEARCH ARTICLE

Control of apico–basal epithelial polarity by the microtubule minus-end-binding protein CAMSAP3 and spectraplakin ACF7

Ivar Noordstra, Qingyang Liu, Wilco Nijenhuis, Shasha Hua, Kai Jiang, Matthijs Baars, Sanne Remmelzwaal, Maud Martin, Lukas C. Kapitein and Anna Akhmanova*

ABSTRACT

The microtubule cytoskeleton regulates cell polarity by spatially organizing membrane trafficking and signaling processes. In epithelial cells, microtubules form parallel arrays aligned along the apico–basal axis, and recent work has demonstrated that the members of CAMSAP/Patronin family control apical tethering of microtubule minus ends. Here, we show that in mammalian intestinal epithelial cells, the spectraplakin ACF7 (also known as MACF1) specifically binds to CAMSAP3 and is required for the apical localization of CAMSAP3-decorated microtubule minus ends. Loss of ACF7 but not of CAMSAP3 or its homolog CAMSAP2 affected the formation of polarized epithelial cysts in three-dimensional cultures. In short-term epithelial polarization assays, knockout of CAMSAP3, but not of CAMSAP2, caused microtubule re-organization into a more radial centrosomal array, redistribution of Rab11-positive (also known as Rab11A) endosomes from the apical cell surface to the pericentrosomal region and inhibition of actin brush border formation at the apical side of the cell. We conclude that ACF7 is an important regulator of apico–basal polarity in mammalian intestinal cells and that a radial centrosome-centered microtubule organization can act as an inhibitor of epithelial polarity.

KEY WORDS: Microtubule, Epithelial cells, Apico–basal polarity, Brush border, Rab11, Endosomes

INTRODUCTION

Microtubules regulate cell polarity by serving as rails for intracellular transport and by controlling organelle positioning and signaling. Although in many types of cultured cells microtubules form a radial array, in polarized epithelial cells, microtubules are arranged along the apico–basal axis, with the minus ends located at the apical side (Akhmanova and Hoogenraad, 2015; Bartolini and Gundersen, 2006; Dammermann et al., 2003). This non-centrosomal microtubule organization can be controlled by the relocalization of γ-tubulin-binding centrosomal microtubule-anchoring proteins, such as ninein, to non-centrosomal apical sites (Moss et al., 2007) and by proteins that bind to microtubule minus ends independently of γ-tubulin. The most notable example of the latter are the members of calmodulin-regulated spectrin-associated protein (CAMSAP)/Patronin family, which can recognize and decorate free microtubule minus ends and protect non-centrosomal microtubules from depolymerization (Goodwin and Vale, 2010; Hendershott and Vale, 2014; Jiang et al., 2014; Tanaka et al., 2012). Recent work in worms has demonstrated that a ninein homolog and Patronin can act both redundantly and non-redundantly in organizing non-centrosomal arrays in different cell types (Wang et al., 2015).

In mammalian cells, the minus-end-binding protein CAMSAP3 (also known as Nezha or Marshalin) was initially shown to interact with components of adherens junctions and to anchor microtubule minus ends at these sites (Meng et al., 2008). CAMSAP3 is also very abundant in supporting cells of the organ of Corti, a specialized type of epithelial cell with extremely dense microtubule bundles that are anchored at centrosomal and non-centrosomal microtubule-organizing centers at the cell cortex (Takahashi et al., 2016; Zheng et al., 2013). Similar to other CAMSAP/Patronin-family members, CAMSAP3 has a C-terminal conserved domain, the CKK, as well as several coiled-coil regions and an N-terminal calponin homology domain, the function of which is currently unknown (Akhmanova and Hoogenraad, 2015; Baines et al., 2009). Through the CKK domain and the adjacent positively charged microtubule-binding regions, CAMSAP3, as well as its homolog CAMSAP2 recognize and decorate polymerizing microtubule minus ends, forming stretches of stabilized microtubule lattice that can serve as 'seeds' for non-centrosomal microtubule outgrowth (Jiang et al., 2014). Recent work shows that CAMSAP3 is an important factor in organizing apico–basal microtubule arrays in enterocytes, where it strongly localizes to the apical cell cortex and tethers microtubule minus ends (Toya et al., 2016). Mice homozygous for the C-terminal truncation of CAMSAP3, in which the CKK domain is lost, are viable but show increased lethality at early postnatal stages (Toya et al., 2016). Intestinal epithelial cells of those mice could still polarize and form a normal brush border, in spite of the fact that the microtubules were disorganized, and the nuclei and Golgi membranes mispositioned (Toya et al., 2016). Experiments in Caco-2 cells, a human intestinal cancer cell line, have demonstrated that the first coiled-coil region of CAMSAP3 is involved in recruitment of CAMSAP3-bound microtubule minus ends to the apical side (Toya et al., 2016). In CAMSAP1, this coiled-coil region was shown to bind to spectrin (King et al., 2014). Whether the apical localization of CAMSAP3, indeed, depends on spectrin or some other proteins has not been determined.

Here, we set out to investigate the mechanism of CAMSAP3 recruitment to the apical side of epithelial cells. We found that CAMSAP3, but not CAMSAP2, interacts with the spectraplakin ACF7 (also known as MACF1; Karakesisoglou et al., 2000; Kodama et al., 2003; Wu et al., 2008) and that ACF7 depletion leads to the release of CAMSAP3-decorated microtubule stretches from the apical cell surface. ACF7, CAMSAP2 and CAMSAP3 were not essential for the distribution of early cell polarity markers in two-dimensional (2D) cultures; however, loss of ACF7 but not of the two CAMSAP proteins affected the formation of epithelial cysts in 3D cultures, indicating that ACF7 plays a more profound role in

Cell Biology, Department of Biology, Faculty of Science, Utrecht University, Padualaan 8, Utrecht 3584 CH, The Netherlands.

*Author for correspondence (a.akhmanova@uu.nl)

A.A., 0000-0002-9048-8614

Received 8 July 2016; Accepted 7 October 2016

Journal of Cell Science (2016) 129, 4278-4288 doi:10.1242/jcs.194878

epithelial polarity than the CAMSAP proteins. Loss of CAMSAP3 led to more centrosome-centered microtubule organization, and this affected the organization of the actin cytoskeleton at the apical side of the cell, probably owing to mislocalization of recycling endosomes that are positive for Rab11A, which are an important component in apical polarity and brush border formation in intestinal cells (Bryant et al., 2010; Dhekne et al., 2014; Knowles et al., 2015; Overeem et al., 2015; Sobajima et al., 2015). Taken together, our study identifies ACF7 as an important regulator of apico–basal polarity in mammalian intestinal cells and demonstrates the importance of non-centrosomal microtubule organization for efficient epithelial cell polarization.

RESULTS

Visualization of localization and dynamics of CAMSAP3 in polarized epithelial cells using GFP-knock-in cells

To facilitate visualization of CAMSAP3 in Caco-2 cells, we have generated a homozygous knock-in line in which the endogenous CAMSAP3 protein was tagged with GFP (Fig. 1A). In agreement with previous publications (Meng et al., 2008; Tanaka et al., 2012; Toya et al., 2016), in this cell line, CAMSAP3–GFP localized to microtubule ends, colocalized with endogenous CAMSAP2 and was concentrated at the apical side of polarized Caco-2 monolayers (Fig. 1B–D). Upon microtubule depolymerization through nocodazole treatment, no apical CAMSAP3 stretches were detected, indicating that the apical recruitment of CAMSAP3 strongly depends on the presence of microtubules (Fig. 1E). We next used fluorescence recovery after photobleaching (FRAP) assays to investigate the turnover of CAMSAP3–GFP at the apical side of polarized Caco-2 monolayers. We found that in 1-day-old Caco-2 monolayers, a ∼75% recovery of CAMSAP3–GFP signals at the apical surface occurred within ∼15 min (Fig. 1F,G). This recovery was associated with movements of unbleached CAMSAP3–GFP-labeled microtubule minus ends into the photobleached area (Fig. 1F,H). Interestingly, ∼15 min after photobleaching in 5-day-old monolayers, the CAMSAP3–GFP signal at the apical surface recovered only to ∼40% (Fig. 1F,G). The mobility of CAMSAP3–GFP stretches in older cultures was much lower (Fig. 1H), indicating that the apical cytoskeleton undergoes maturation on a scale of several days, resulting in immobilization of CAMSAP3 stretches.

When Caco-2 cells were cultured in Matrigel, they formed cysts, as described previously (Jaffe et al., 2008). Already at the two-cell stage, GFP–CAMSAP3 colocalized with apical markers, such as atypical protein kinase C (aPKC), and the area of enhanced actin accumulation, which was located at the membrane interface between the two daughter cells, as shown previously (Jaffe et al., 2008) (Fig. 1I). After 4 days in 3D culture, GFP–CAMSAP3 strongly accumulated at the apical side (Fig. 1J). In such polarized cysts, microtubules were aligned along the apico–basal axis (Fig. 1K).

We never observed any accumulation of GFP–CAMSAP3 at the cell–cell junctions in either 2D or 3D cultures, which is in line with the observations in mouse intestine but contradicts the data previously obtained by immunostaining of CAMSAP3 in Caco-2 cells (Meng et al., 2008; Toya et al., 2016). Our data are thus in full agreement with the role of CAMSAP3 in apical microtubule organization but provide no support for CAMSAP3 function at the adherens junctions.

ACF7 binds to CAMSAP3 and participates in its apical recruitment

We reasoned that the capture and stable association of CAMSAP3 stretches at the apical surface is caused by the presence of a binding partner. To identify CAMSAP3-interacting proteins, we performed streptavidin pull-down assays from HEK293T cells that co-expressed biotinylation (Bio) and GFP-tagged CAMSAP3 and the biotinylated ligase BirA, and analyzed the isolated proteins by performing mass spectrometry (Jiang et al., 2014). The highest scoring hit in this screen was the spectraplakin ACF7 (Fig. 2A), whereas no peptides that were derived from spectrin, which has been previously reported to bind to CAMSAP1 (King et al., 2014), were found. Whether this was owing to the absence of appropriate spectrin isoforms in HEK293T cells, the biochemical procedure used or the lack of interaction between CAMSAP3 and spectrin is unclear.

Immunostaining showed colocalization of GFP–CAMSAP3 with the puncta of endogenous ACF7 at the apical side of Caco-2 monolayers (Fig. 2B). However, in contrast to CAMSAP3, which was only located apically, ACF7 was spread throughout the cytoplasm (Fig. 2D). As an alternative model of enterocyte polarity, we used the LS174T-W4 cell line, in which the activation of LKB1 kinase through doxycycline-induced expression of the adapter protein STRAD (also known as STRADA) is sufficient to induce polarization and formation of microvilli on one side of the cell in the absence of cell–cell contacts (Baas et al., 2004). In doxycycline-treated LS174T-W4 cells, both endogenous and GFP-tagged CAMSAP3 colocalized with endogenous ACF7 beneath the polarized regions of actin enrichment (Fig. 2C), supporting complex formation between CAMSAP3 and ACF7.

We next investigated the interaction between CAMSAP3 and ACF7 biochemically. ACF7 is a very large protein (∼5000 amino acids) containing an N-terminal actin-binding calponin homology domain, a plakin domain, 30 spectrin repeats, EF-hand motifs that could mediate Ca^{2+} binding, a microtubule-binding GAS2-related domain and the EB1-binding SxIP motif (Karakesisoglou et al., 2000; Kodama et al., 2003; Wu et al., 2008) (Fig. 2E). Because the full-length ACF7 is difficult to efficiently express in cells, we generated GFP-tagged ACF7 fragments covering the whole ACF7 protein. We performed streptavidin pull-down assays from HEK293T cells co-expressing these fragments together with biotin ligase BirA and CAMSAP2 or CAMSAP3 tagged with an mCherry and biotinylation tag (Bio–mCherry), or just the Bio–mCherry protein as a negative control. We found that CAMSAP3, but not CAMSAP2, specifically bound to the ACF7 fragment encompassing spectrin repeats 20–26 (fragment ACF7_5, Fig. 2F). Deletion mapping further showed that the coiled-coil region 1 (CC1) of CAMSAP3, which has been previously implicated in the apical localization of the protein (Toya et al., 2016), was essential for this interaction (Fig. 2G).

The binding between CAMSAP3 and ACF7 was confirmed by performing colocalization experiments in HeLa cells. Overexpression of CAMSAP3 and CAMSAP2 caused strong bundling of microtubules, and CAMSAP3, but not CAMSAP2, could specifically recruit fragment ACF7_5 to these microtubule bundles (Fig. 2H). Furthermore, we found that endogenous ACF7 was recruited to microtubule bundles that had been induced through overexpression of full-length CAMSAP3 and of the CAMSAP3 deletion mutant that lacked the calponin homology domain, but not of the CAMSAP3 deletion mutants that lacked the CC1 region (Fig. S1). Taken together, these data indicate that CAMSAP3 and ACF7 interact with each other and can cooperate in binding to microtubules. Deletion mapping showed that the CC1 region of CAMSAP3 and a specific spectrin-repeat region of ACF7 are required for the interaction.

Journal of Cell Science (2016) 129, 4278-4288 doi:10.1242/jcs.194878

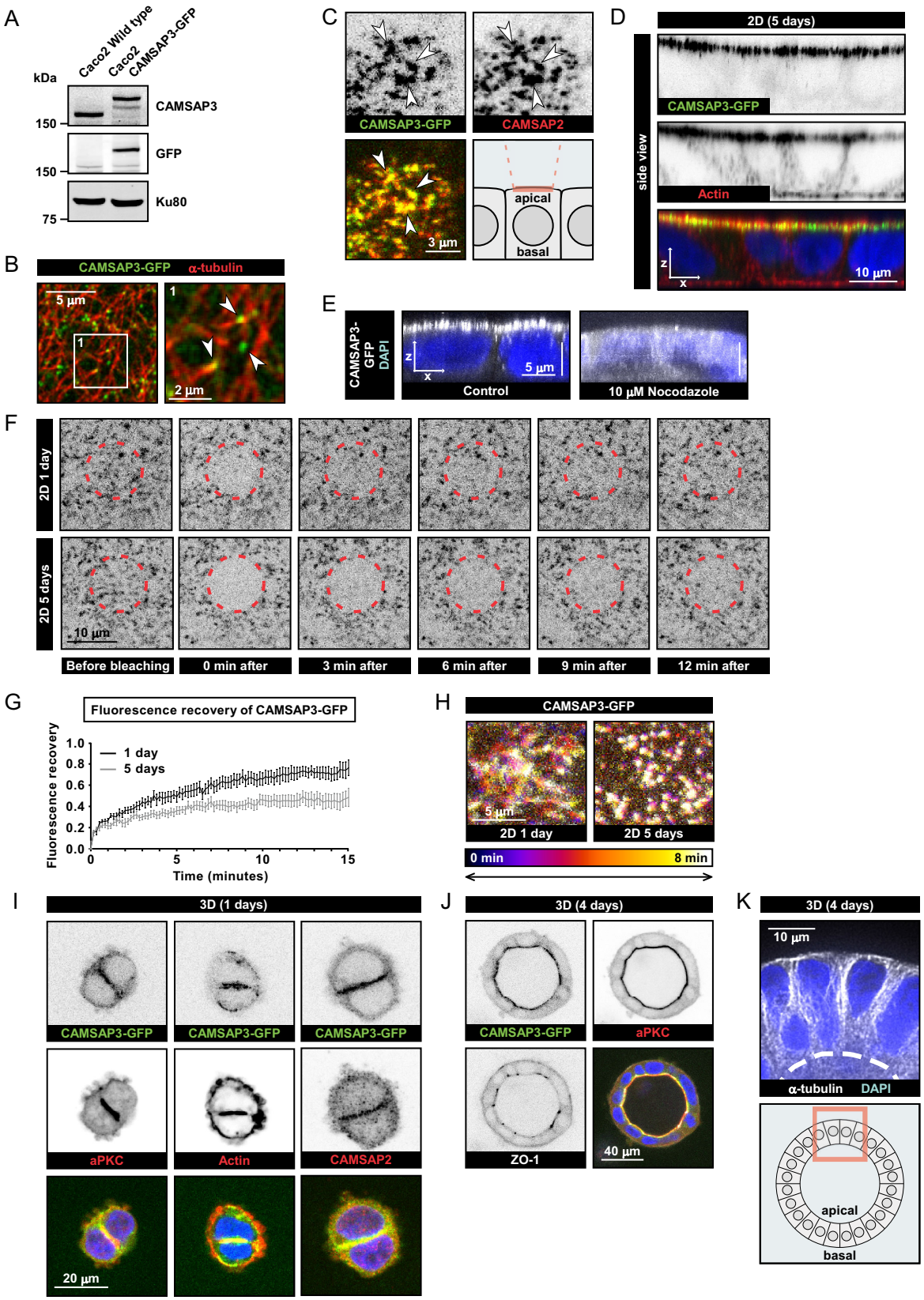

Fig. 1. See next page for legend.

We next investigated whether ACF7 participates in the apical recruitment of CAMSAP3. ACF7 was depleted with two different small interfering (si)RNAs, and the efficiency of depletion was confirmed by immunofluorescence staining and real-time PCR (Fig. 3A–C). Although actin enrichment was still observed at the apical side of ACF7-depleted Caco-2 monolayers, both the apical

Journal of Cell Science

Journal of Cell Science (2016) 129, 4278-4288 doi:10.1242/jcs.194878

Fig. 1. Visualization of localization and dynamics of CAMSAP3 in polarized epithelial cells using CAMSAP3–GFP knock-in cells. (A) Western blot analysis of extracts of wild-type and CAMSAP3–GFP knock-in Caco-2 cells. (B) Staining for α-tubulin (red) in CAMSAP3–GFP (green) knock-in Caco-2 cells. White arrowheads indicate CAMSAP3 signal at microtubule ends. The area imaged is indicated in the schematic in C. (C) Staining of CAMSAP2 (red) in CAMSAP3–GFP (green) knock-in Caco-2 cells. White arrowheads indicate the same positions in different panels. Image area is indicated by red rectangle in the scheme. (D) Side view of CAMSAP3–GFP (green) knock-in Caco-2 monolayer stained for actin (red) and DNA (blue). (E) Side view of control and nocodazole-treated CAMSAP3–GFP (white) knock-in Caco-2 monolayers stained for DNA (blue). (F) FRAP analysis of CAMSAP3–GFP at the apical side of a Caco-2 monolayer either 1 or 5 days after reaching a confluent state. Red circle indicates photobleached region. The area imaged is indicated in the schematic in C. (G) Average normalized fluorescence intensity graphs after photobleaching as described in E. Error bars, s.e.m. (H) Motility representation of CAMSAP3–GFP stretches. Images are presented as maximum projections of 8-min movies with an interval of 10 s (48 frames). Image colors indicate time points (see gradient). The area imaged is indicated in the schematic in C. (I) Staining for actin, aPKC, CAMSAP2 (red) and DNA (blue) in 1-day-old 3D cultures of CAMSAP3–GFP (green) knock-in Caco-2 cells. (J) Staining of aPKC (red), ZO-1 (white) and DNA (blue) in 4-day-old 3D cultures of CAMSAP3–GFP (green) knock-in Caco-2 cells. (K) Staining for α-tubulin (white) and DNA (blue) in 4-day-old 3D cultures of Caco-2 cells. Apical cell surface is indicated by a white stippled line. Image area is indicated by a red square in the scheme.

localization and the total number of CAMSAP3–GFP stretches were very strongly reduced, indicating that ACF7 regulates the localization as well as the formation or stability of CAMSAP3-decorated microtubule stretches (Fig. 3D,E). In contrast, other early polarity markers, such as ezrin, aPKC and zonula occludens 1 (ZO-1; also known as TJP1) were still apically located in 2D cultures of ACF7-depleted cells (Fig. 3D; Fig. S2A). Also, the height of polarized monolayers was not significantly affected in the absence of ACF7 (Fig. S2B). Further, in line with the fact that ACF7 depletion reduced the abundance of CAMSAP3-decorated microtubule stretches, we found an increase, albeit a mild one, in the number of centrosomal microtubules, indicating that ACF7 contributes to some extent to the maintenance of a non-centrosomal microtubule network (Fig. S2C,D).

To further address the effect of ACF7 knockdown, we analyzed cyst formation in 3D cultures. To accelerate lumen formation in Caco-2 cysts in order to make 3D analysis compatible with a transient protein depletion protocol, we used dense Caco-2 3D cultures and, after the initial cyst formation, treated them with cholera toxin, which strongly stimulates lumen formation by inducing cAMP signaling (Jaffe et al., 2008). Under these conditions, we found a clear well-formed or mildly disorganized lumen in ∼75% of cysts that had been treated with control siRNAs, whereas after ACF7 depletion, only 10% of the cysts developed normally, and cysts completely lacking the lumen were prevalent (Fig. 3F,G). Analysis of early (3–4 cell) 3D cultures showed that although the apical polarity markers localized to intercellular junctions in control cells, as described previously (Jaffe et al., 2008), they were mislocalized in ACF7-knockdown cells (Fig. 3H).

We conclude that although ACF7 depletion does not cause mislocalization of all polarity markers in 2D cultures, it does lead to the loss of apical localization of CAMSAP3. When embedded in a 3D matrix, the distribution of all investigated polarity markers and cyst formation were strongly affected by ACF7 depletion, indicating that distinct mechanisms with differential sensitivities to ACF7 levels control the ability of cells to polarize in 2D and 3D cultures.

CAMSAP3 knockout leads to Rab11A mislocalization and inhibition of apical actin brush border formation

We next set out to address the effects of the loss of CAMSAP2 and CAMSAP3 on epithelial polarity. Using CRISPR-Cas9 technology, we knocked out CAMSAP2 or CAMSAP3 genes in the CAMSAP3-GFP knock-in cell line (Fig. 4A,B). Apical CAMSAP3–GFP signals were unperturbed in CAMSAP2-knockout cells, whereas in CAMSAP3-knockout cells, CAMSAP2 stretches became longer, as described previously (Tanaka et al., 2012) (Fig. 4A). CAMSAP-decorated microtubule stretches are generated through microtubule polymerization from the minus end, and the stretches formed in the presence of CAMSAP3 and CAMSAP2 are likely to be shorter than those formed in the presence of CAMSAP2 alone, because CAMSAP3 is a more efficient inhibitor of microtubule minus-end growth than CAMSAP2 (Jiang et al., 2014). Microtubule organization was not visibly changed in CAMSAP2-knockout cells, but a more centrosome-centered array was observed in CAMSAP3-knockout cells, in line with the findings of a previous study (Tanaka et al., 2012) (Fig. 4C,D).

Next, we analyzed polarity in CAMSAP2- and CAMSAP3-knockout clones. In 2D cultures, junctional ZO-1 and E-cadherin, as well as the early markers of apical polarity aPKC and ezrin, were unperturbed (Fig. S3A,B). When cultured in 3D, two out of three CAMSAP2-knockout clones and three out of three CAMSAP3-knockout clones formed morphologically normal cysts (Fig. S3C, D). Because two CAMSAP2-knockout lines could form morphologically normal cysts, we think that the morphological abnormalities in the third clone were due to secondary mutations. This conclusion was confirmed by siRNA-mediated depletion of CAMSAP2, CAMSAP3 or both CAMSAPs simultaneously (Fig. S3E). In addition, CAMSAP2- and CAMSAP3-knockout clones showed no defects in the recruitment of the apical markers aPKC and ZO-1 in early 3D cysts (Fig. S3F). We conclude that CAMSAP2 and CAMSAP3 are not required for the formation of lumen-containing 3D cysts, indicating that the strongly affected cyst formation in ACF7-depleted cells is unlikely to be due to CAMSAP3 mislocalization.

We then focused on late markers of epithelial polarity that are associated with the ability of the cells to form a brush border. Apical accumulation of actin and the phosphorylated form of ezrin, an actin-binding protein important for the formation of brush border (Dhekne et al., 2014; Overeem et al., 2015; Viswanatha et al., 2012) was unaffected in CAMSAP2-knockout cells (Fig. 4E,F; Fig. S3A), even though the same cell line showed abnormalities in cyst morphology in 3D culture (Fig. S3C,D; CAMSAP2 KO #1). This result indicates that the ability of cells to form 3D cysts and to localize actin regulators does not necessarily correlate.

Strikingly, in CAMSAP3-knockout cells, the apical accumulation of actin and phosphorylated ezrin was concentrated around the cell–cell junctions and reduced in the central part of the cell (Fig. 4E,F; Fig. S3A). Previous work has shown that during brush border formation, the apical actin cytoskeleton is strongly regulated by signaling and/or trafficking processes that are dependent on the apical accumulation of Rab11A-positive recycling endosomes (Dhekne et al., 2014; Knowles et al., 2015; Overeem et al., 2015; Sobajima et al., 2015). We analyzed the distribution of Rab11A endosomes by using cells that had been stably transfected with a construct for doxycycline-inducible expression of dTomato–Rab11A. Strikingly, in control and CAMSAP2-knockout cells, Rab11A endosomes were distributed under the apical surface, whereas in CAMSAP3-knockout cells they displayed a single focus of accumulation, which coincided with the

Journal of Cell Science (2016) 129, 4278-4288 doi:10.1242/jcs.194878

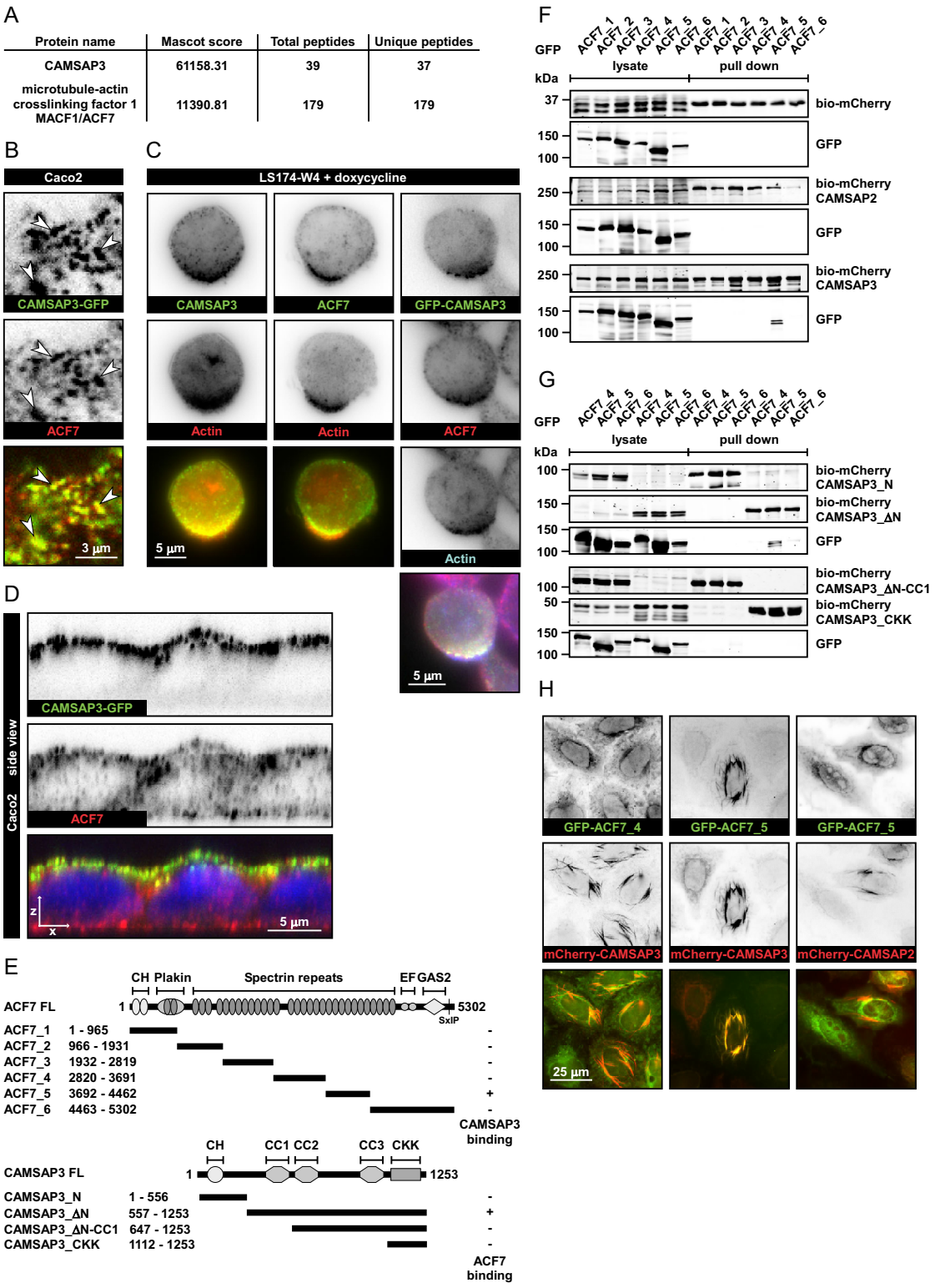

Fig. 2. CAMSAP3 interacts with ACF7. (A) Identification of ACF7 as a binding partner of CAMSAP3 by mass-spectrometry-based analysis of a streptavidin pull-down assay with the extracts of HEK293T cells expressing biotinylation-tagged CAMSAP3 and BirA. (B) Staining of ACF7 (red) in CAMSAP3–GFP (green) knock-in Caco-2 cells. White arrowheads indicate the same positions in different panels. The area imaged is indicated in Fig. 1C. (C) Staining of different markers in polarized LS174-W4 cells after doxycycline treatment. Left column, staining of CAMSAP3 (green) and actin (red); middle column, staining of ACF7 (green) and actin (red); right column, staining of ACF7 (red) and actin (blue) in a GFP–CAMSAP3-expressing cell. (D) Side view of CAMSAP3–GFP (green) knock-in Caco-2 monolayer stained for ACF7 (red) and DNA (blue). (E) Domain organization of ACF7 and CAMSAP3, and the deletion mutants used to study protein binding sites and a summary of experimental results indicating protein interactions. FL, full length; CH, calponin homology domain; EF, EF-hand; GAS2, growth-arrest-specific protein 2 domain; CC, coiled-coil domain. (F) Streptavidin pull-down assays from HEK293T cells expressing different GFP-tagged ACF7 fragments, BirA and Bio–mCherry, Bio–mCherry–CAMSAP2 or Bio–mCherry–CAMSAP3. (G) Streptavidin pull-down assays from HEK293T cells expressing different GFP-tagged ACF7 fragments, BirA and different Bio–mCherry-tagged CAMSAP3 fragments. (H) Transiently transfected HeLa cells co-expressing GFP–ACF7 fragments (green) and mCherry–CAMSAP2 or mCherry–CAMSAP3 (red).

Journal of Cell Science

Journal of Cell Science (2016) 129, 4278-4288 doi:10.1242/jcs.194878

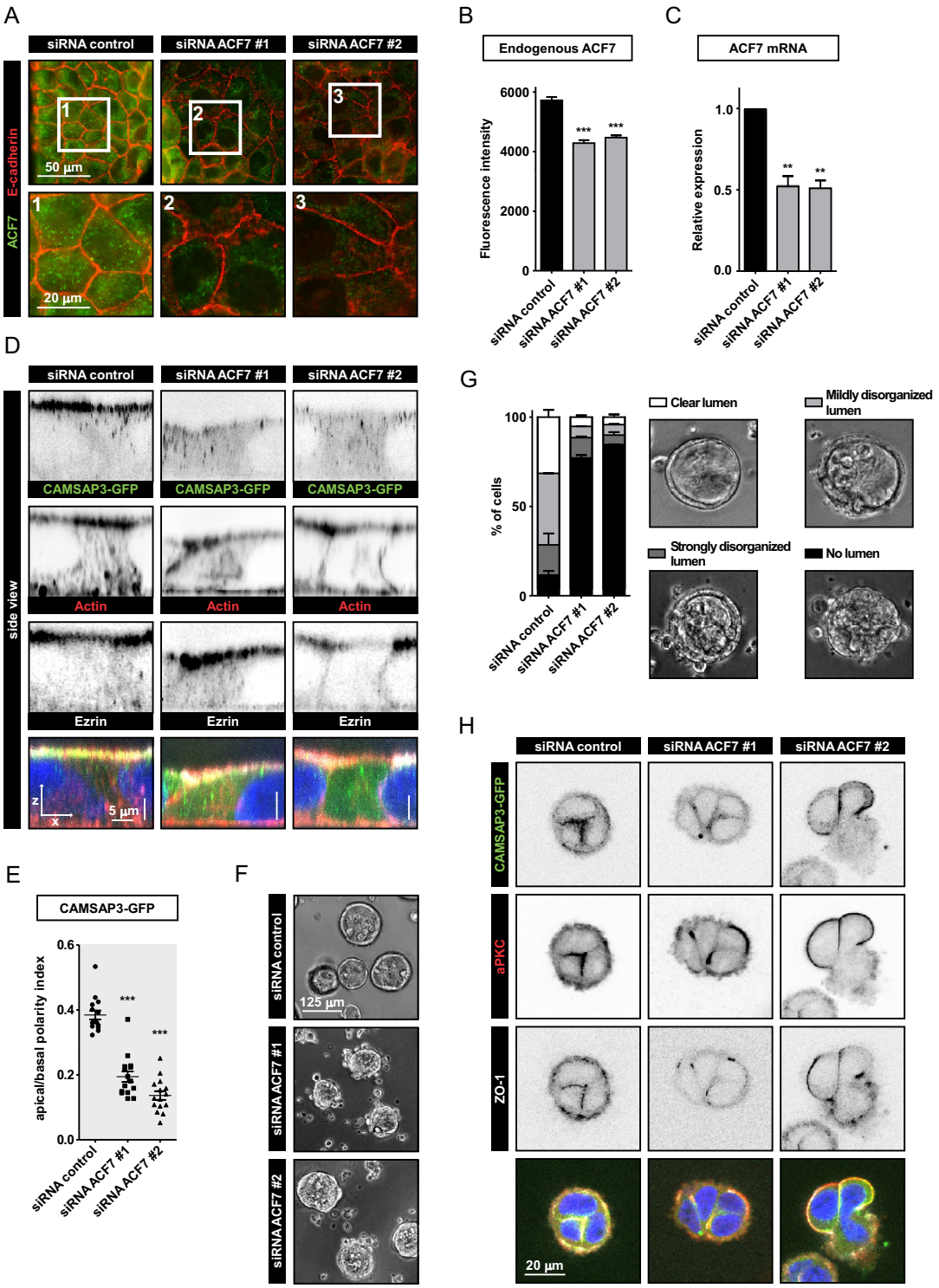

Fig. 3. Knockdown of ACF7 perturbs epithelial polarity and CAMSAP3 distribution. (A) Staining of ACF7 (green) and E-cadherin (red) in Caco-2 cells transfected with control siRNA or siRNA against ACF7. (B) Quantification of fluorescence intensity of endogenous ACF7 staining in cells treated as described in A. siRNA control, n=78; siRNA ACF7 #1, n=73; siRNA ACF7 #2, n=63; ***P<0.001; Mann–Whitney U-test; error bars, s.e.m. (C) qPCR analysis of ACF7 mRNA expression in cells treated as described in A. ACF7 expression was calculated relative to that under the control condition using two different primer pairs and after normalization to two housekeeping genes. siRNA control, n=12; siRNA ACF7 #1, n=12; siRNA ACF7 #2, n=12; **P<0.01; paired t-test; error bars, s.e.m. (D) Side view of CAMSAP3–GFP (green) knock-in Caco-2 monolayer stained for actin (red), ezrin (white) and DNA (blue) and transfected with siRNAs as described in A. (E) Quantification of CAMSAP3–GFP localization presented as the apical–basal polarity index [(apical fluorescence intensity/basal fluorescence intensity)−1]. Cells were transfected with siRNAs as described in A. siRNA control, n=15; siRNA ACF7 #1, n=15; siRNA ACF7 #2, n=15; ***P<0.001; Mann–Whitney U-test. Single data points are plotted. Horizontal line, mean; error bars, s.e.m. (F) 3D cyst formation 1 day after dense seeding of Caco-2 cells treated as described in A. (G) Quantification of 3D cyst formation of cells shown in F. siRNA control, n=200; siRNA ACF7 #1, n=236; siRNA ACF7 #2, n=139; error bars, s.e.m. (H) Staining of aPKC (red), ZO-1 (white) and DNA (blue) in CAMSAP3–GFP (green) knock-in Caco-2 cells seeded in a 3D matrix and transfected with siRNA as described in A.

Journal of Cell Science (2016) 129, 4278-4288 doi:10.1242/jcs.194878

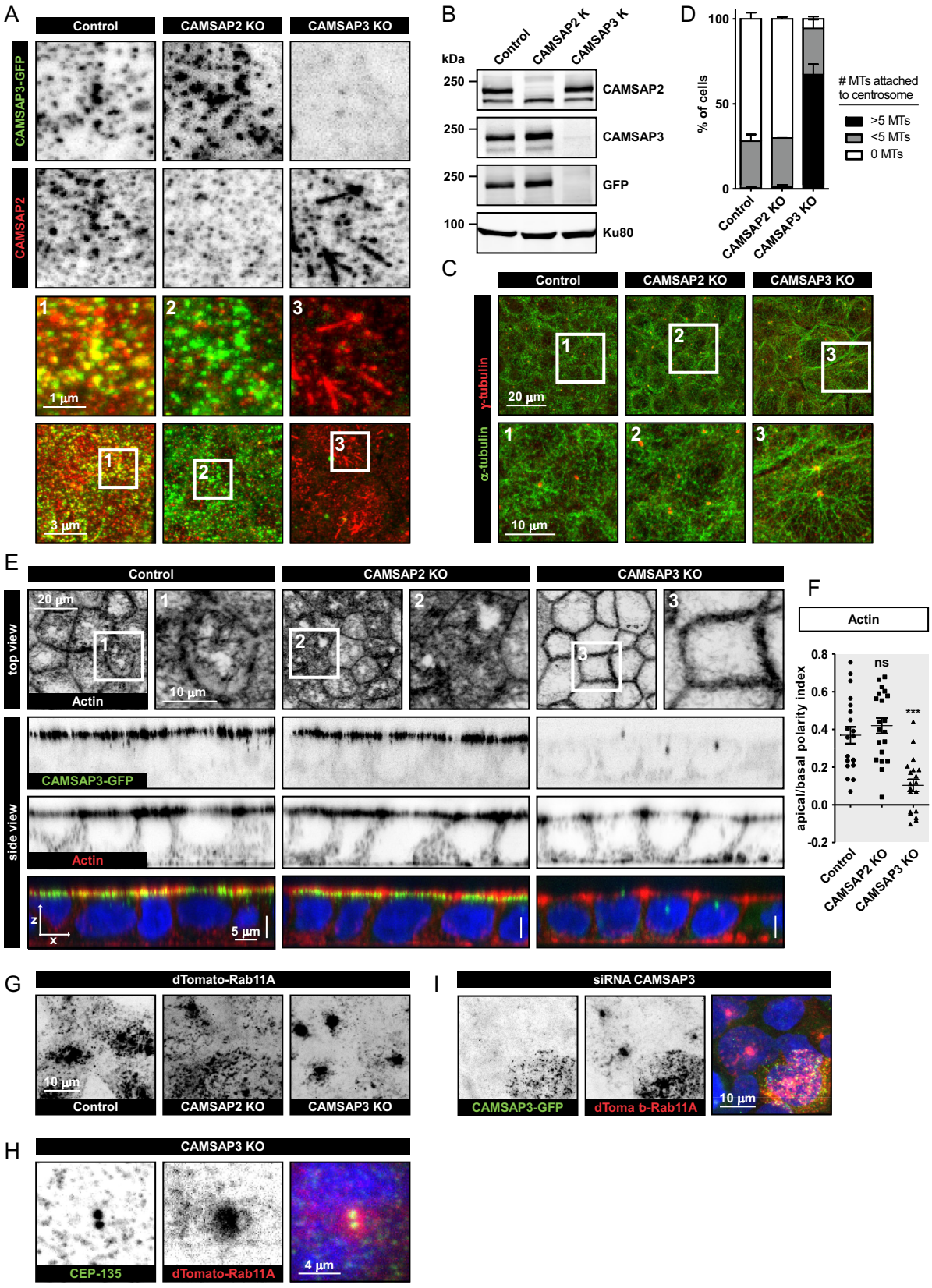

Fig. 4. See next page for legend.

centrosome (Fig. 4G,H; Fig. S3G). In fact, the fluorescence intensity of the Rab11A clusters in CAMSAP3-knockout cells appeared to be ∼5-fold higher than the fluorescence intensity of apically located Rab11A vesicles in control cells, revealing a very strong clustering of endosomes (Fig. S3G). This result was confirmed in cells in which CAMSAP3 had been depleted using

Fig. 4. Knockout of CAMSAP3 perturbs the distribution of Rab11A-positive endosomes and apical actin organization. (A) CAMSAP3–GFP (green, knock-in) and CAMSAP2 (red, staining) in control, and CAMSAP2- and CAMSAP3-knockout (KO) cells. (B) Western blot analysis of control, and of CAMSAP2- and CAMSAP3-knockout cell extracts. (C) Staining of microtubules (green, α-tubulin) and centrosomes (red, γ-tubulin) in the control and knockout cells described in A. (D) Quantification of microtubule organization, presented as the number of microtubules attached to the centrosome. Quantification is based on the staining shown in C. Numbers of analyzed cells: control, *n*=196; CAMSAP2 KO, *n*=195; CAMSAP3 KO, *n*=122; error bars, s.e.m.; #, number; MTs, microtubules. (E) Top view: staining of actin in the control or knockout cells shown in A. Side view: side view of a monolayer of control or knockout cells described in A showing CAMSAP3–GFP knock-in, (green), actin (red, staining) and DNA (blue, staining). (F) Quantification of actin localization presented as the apical–basal polarity index [(apical fluorescent intensity/basal fluorescent intensity)−1] in the control or knockout cells described in A. Control, *n*=20; CAMSAP2 KO, *n*=20; CAMSAP3 KO, *n*=20; ***$P<0.001$; ns, no significant difference with control; Mann–Whitney *U*-test. Single data points are plotted. Horizontal line, mean; error bars, s.e.m. (G) Distribution of endosomes visualized with stably expressed dTomato–Rab11A in the control and knockout cells described in A. (H) Staining of centrosomes (CEP135, green) in dTomato–Rab11A-expressing CAMSAP3-knockout cells. (I) CAMSAP3–GFP (green, knock-in) and dTomato–Rab11A (red, stably expressed) in Caco-2 cells transfected with siRNA against CAMSAP3.

siRNA: in these cells, the formation of a single centrally located Rab11A cluster strongly correlated with the efficiency of CAMSAP3 knockdown (Fig. 4I). We also analyzed Rab11A in ACF7-knockdown cells and found that the endosomes were equally distributed over the cell, indicating defects in the apical targeting (Fig. S3G). However, actin still accumulated at the apical surface of ACF7-depleted cells (Fig. 3D), suggesting that clustering of Rab11A endosomes in the middle part of the cell is more deleterious for actin organization than their random distribution.

Our data support the notion that the localization of Rab11A endosomes strongly correlates with the position of microtubule minus ends, in line with the idea that it is controlled by cytoplasmic dynein (Horgan et al., 2010; Khanal et al., 2016; Riggs et al., 2007). When the microtubule array becomes more radial, Rab11A endosomes accumulate in the central part of the cell, and the formation of apical actin-rich structures is inhibited.

DISCUSSION

In this study, we showed that the spectraplakin ACF7 is a binding partner of CAMSAP3 and that it is required for regulating the abundance and apical localization of CAMSAP3-decorated microtubule stretches. While this paper was in preparation, the *Drosophila* homologues of CAMSAP3 and ACF7, Patronin and Shortstop (Shot), respectively, were demonstrated to be present in the same apical complex and cooperate with each other, as well as an apical form of spectrin, in organizing apico–basal microtubule arrays in fly epithelia (Khanal et al., 2016) and in early fly embryos (Nashchekin et al., 2016). These findings are also consistent with earlier work in flies, which has demonstrated the importance of Shot for microtubule minus-end organization during tubulogenesis of the embryonic salivary glands (Booth et al., 2014). ACF7 appears to act upstream of CAMSAP3 as a cortical recruitment factor but, given that it has a microtubule-interacting domain, it is also likely to synergize with CAMSAP3 to some extent for microtubule binding and stabilization. We note that the accumulation of CAMSAP3 at the apical cortex occurred in the form of microtubule stretches and thus depended on the presence of intact microtubules. This is similar to the recruitment of CAMSAP2 to the Golgi membranes, where binding of CAMSAP2-decorated microtubule minus ends but not of the cytosolic CAMSAP2 was observed (Wu et al., 2016). It is possible that the presence of multiple CAMSAP molecules on the same microtubule is required for efficient binding to intracellular structures such as the Golgi and the actin-rich cortex by increasing avidity.

Because ACF7 does not show an exclusively apical localization in Caco-2 cells, an additional pathway ensuring tethering of CAMSAP3-decorated stretches specifically to the apical surface must exist. It is possible that, similar to flies, a specific apical isoform of spectrin might be involved; this would mean that the same region of CAMSAP3, the CC1, mediates apical localization by binding to two different proteins. Alternatively, some signaling pathway restricting CAMSAP3 binding to microtubules at the apical cell side might be involved. Interesting in this respect is our observation that CAMSAP3-decorated microtubule stretches become less mobile during monolayer maturation, suggesting that as epithelial cells differentiate, more numerous connections between these stretches and the cortical cytoskeleton are formed, or the cortical cytoskeleton itself becomes less dynamic. It is also important to note that analysis of 3D cysts showed that ACF7 depletion has a stronger impact on cell polarity than loss of CAMSAP proteins, indicating that ACF7 performs additional CAMSAP-independent functions during epithelial polarization.

Furthermore, our data showed that the knockout of CAMSAP3 affected apical actin organization, probably because the more centrosomal microtubule system in CAMSAP3-knockout cells prevents apical accumulation of Rab11A endosomes. How can these results be reconciled with the presence of a normal brush border in mice expressing nonfunctional CAMSAP3 (Toya et al., 2016)? The most likely explanation is the gradual centrosome inactivation observed during long-term differentiation of epithelial cells. In line with this idea, in CAMSAP3-knockout mice, microtubules in epithelial cells become disorganized but do not form a radial pattern (Toya et al., 2016). A disorganized non-centrosomal array is likely to delay but not to block apical localization of Rab11A endosomes or other yet unknown polarity factors that are transported towards microtubule minus ends. In contrast, the presence of a centrosome seems to act in a dominant-negative manner, by sequestering these factors in the central part of the cell. In line with this idea, actin accumulation at the apical side was inhibited more strongly in CAMSAP3-knockout cells, in which Rab11A endosomes were clustered, than in ACF7-knockdown cells, in which the endosomes were distributed throughout the cell. These data suggest that although the centrosome can promote cell polarization under certain conditions (Bornens, 2012), in epithelial cells it acts as a polarity inhibitor and its microtubule-anchoring activity must be suppressed to allow the cells to efficiently complete their polarization program.

MATERIALS AND METHODS

Cell culture and transfection

Caco-2 cells were obtained from Alpha Yap (University of Queensland, Australia) (Ratheesh et al., 2012) and cultured in Dulbecco's modified Eagle's medium supplemented with 10% fetal calf serum (FCS). LS174-W4 cells (Baas et al., 2004) were obtained from Johannes L. Bos (UMC Utrecht, The Netherlands) and cultured in RPMI supplemented with 10% FCS. HEK293T cells were obtained from American Type Culture Collection (ATCC) and cultured in DMEM supplemented with 10% FCS. The cell lines were routinely checked for mycoplasma contamination using LT07-518 Mycoalert assay (Lonza). The identity of the cell lines was monitored by immunofluorescence-staining-based analysis with multiple markers. To grow a polarized monolayer of epithelial cells, Caco-2 cells were cultured for 5 days after reaching a fully confluent monolayer. 3D cultures of Caco-2

Journal of Cell Science (2016) 129, 4278-4288 doi:10.1242/jcs.194878

cells were generated by seeding cells on top (lumen formation assay) or within (3D immunofluorescence staining) 9.7 mg/ml Matrigel (Corning). One day after seeding, cells were treated with 100 ng/ml cholera toxin (Sigma-Aldrich).

FuGENE 6 (Promega) was used to transfect different plasmids into Caco-2 and LS174T-W4 cells. Polyethylenimine (PEI, Polysciences) was used to transfect HEK293T cells for streptavidin pull-down assays. HiPerFect (Qiagen) was used to transfect Caco-2 cells with siRNAs at 20 nM. Corresponding experiments were performed 72 h after siRNA transfection.

Streptavidin pull-down assays, western blotting and mass spectrometry

Streptavidin pull down and western blotting were performed as described previously (Jiang et al., 2014). Samples were prepared from pull-down assays of biotinylated proteins from extracts of transfected HEK293T cells using streptavidin beads, as described previously (Jiang et al., 2014), and were resuspended in 10% formic acid with 5% DMSO and were analyzed with an Agilent 1290 Infinity (Agilent Technologies) liquid chromatography instrument, operating in reverse-phase (C18) mode, coupled to a TripleTOF 5600 (AB Sciex) spectrometer. Mass spectrometry spectra (350–1250 *m*/*z*) were acquired in high-resolution mode (R>30,000), whereas tandem mass spectrometry (MS2) spectra were acquired in high-sensitivity mode (R>15,000). Raw files were processed using Proteome Discoverer 1.4 (version 1.4.0.288, Thermo Scientific, Bremen, Germany). The database search was performed using Mascot (version 2.4.1, Matrix Science, UK) against a SwissProt database (taxonomy human). Carbamidomethylation of cysteines was set as a fixed modification and oxidation of methionine was set as a variable modification. Trypsin was specified as the enzyme and up to two missed cleavages were allowed. Data filtering was performed using percolator, resulting in 1% false discovery rate (FDR). Additional filters were: search engine rank 1, peptide confidence high and ion score >20.

Generation of Caco-2 knock-in and knockout lines

Caco-2 CAMSAP3–GFP knock-in in CAMSAP-knockout cells were generated by using CRISPR–Cas9 technology (Ran et al., 2013). The Caco-2 CAMSAP3–GFP knock-in line was generated by transfecting the cells with the pSpCas9(BB)-2A-Puro (PX459) vector (Addgene, #62988) bearing the appropriate targeting sequence (5′-ACCGCCCGGGTGGGG-CTATT-3′) and the donor plasmid. Caco-2 CAMSAP-knockout cell lines were generated by transfecting the cells with PX459 vector bearing appropriate targeting sequences (CAMSAP2: 5′-CATGATCGATACCCTCAT-GA-3′; CAMSAP3: 5′-GTACGATTTCTCGCGGGCCA-3′).

To establish clonal stable knock-in and knockout lines, cells were subjected to selection with 20 µg/ml puromycin for 3 days. After selection, cells were allowed to recover in normal medium for 5 days, and the efficiency of knock-in or knockout was checked by immunofluorescence staining. Depending on the efficiency, 20–100 individual clones were isolated and characterized by immunofluorescence staining.

Protein domain prediction, constructs and siRNAs

Protein domains were predicted using the web-based simple modular architecture research tool (SMART) (Letunic et al., 2015; Schultz et al., 1998). Full-length ACF7 was purchased from Promega Kazusa Genome Technologies (pFN21AE0600). ACF7 constructs were amplified by performing PCR and cloned into pEGFP-C2 (Clontech). Bio–mCherry–CAMSAP2, bio–mCherry–CAMSAP3 and GFP–CAMSAP3 have been described previously (Jiang et al., 2014). Deletion mutants were cloned by using PCR-based strategies.

Gibson assembly was used to assemble a pUC19-based CAMSAP3–GFP knock-in donor plasmid. Primers used to amplify the 5′ homology arm were: 5′-CCTTGGCCCCTCTGCACATA-3′ and 5′-TTTGGGGGTGCCGCCG-CC-3′. Primers used to amplify the 3′ homology arm were: 5′-CCCCAC-CCGGGCGGTCCA-3′ and 5′-TTAGTCCTAAGCCTGGGAAGC-3′.

pSIN-TRE-rtTA-IRES-Hygro-iLID-dTomato-Rab11A was constructed from pSIN-TRE-rtTA-IRES-Puro (kindly provided by Benjamin Bouchet, Utrecht University, The Netherlands) by replacing the puromycin-resistance cassette with the hygromycin-resistance cassette from pCDNA5-FRT-TO (Invitrogen) and encodes amino acids 2–216 human Rab11A (derived from GFP–Rab11A WT, a gift from Richard Pagano, Mayo Clinic College of Medicine, Rochester, MN; Addgene plasmid #12674), N-terminally fused to the light-sensitive dimerization module iLID (derived from pLL7.0: Venus-iLID-Mito, a gift from Brian Kuhlman, University of North Carolina, Chapel Hill, NC; Addgene plasmid #60413) and dTomato.

siRNAs targeting the following sequences were purchased from Sigma-Aldrich: ACF7 #1, 5′-TTGCAGCAGGTGAATGGAC-3′; ACF7 #2, 5′-CCAAAGTGACTTGAAGGAT-3′ (Drabek et al., 2006); CAMSAP2, 5′-GTACTGGATAAATAAGGTA-3′ (Jiang et al., 2014); CAMSAP3, 5′-GCATTCTGGAGGAAATTGA-3′; and control targeting luciferase, 5′-CGTACGCGGAATACTTCGA-3′ (Dambournet et al., 2011).

Antibodies, drugs and chemicals

Rat monoclonal antibody against tyrosinated α-tubulin (clone YL1/2) was purchased from Abcam (#ab6160). Mouse polyclonal antibody against ACF7 was purchased from Abnova (#H00023499-A01). Mouse monoclonal antibodies against the following proteins were used: CAMSAP3 (#SAB4200415) and γ-tubulin (#T5326) (Sigma-Aldrich); Ku80 (#611360), ZO-1 (#610966), E-cadherin (#610181), mCherry (#632543) (Clontech) and ezrin (#610602) (BD Biosciences). Rabbit polyclonal antibodies against the following proteins were used: GFP (#ab290, Abcam); CAMSAP2 (#NBP1-21402 Novus, #17880-1-AP Proteintech); aPKC (#H00023499-A01, Santa Cruz); Actin (#20-33) and CEP135 (#SAB4503685) (Sigma-Aldrich); phosphorylated ERM (#3141, Cell Signaling); E-cadherin (Alpha Yap, University of Queensland, Australia). Alexa-Fluor-405- (#A-31553 and #A-31556), Alexa-Fluor-488- (#A27023 and #A-11034), Alexa-Fluor-594- (#A-11032, #R37117 and #A-11007) and Alexa-Fluor-647- (#A-21235) conjugated goat antibodies against mouse, rabbit and rat were purchased from Life Technologies. For Western blotting, IRDye-800CW-conjugated goat antibody against mouse and rabbit IgG (#P/N 925-32210 and #P/N 925-32211) and IRDye-680LT-conjugated goat antibody against mouse and rabbit IgG (#P/N 925-68020 and #P/N 925-68021) were purchased from Li-Cor Biosciences. See Table S1 for the antibody dilutions used.

Alexa-Fluor-594-conjugated phalloidin was purchased from Life Technologies (#A12381). Doxycycline was purchased from Sigma-Aldrich and used at a concentration of 1 µg/ml. Nocodazole was purchased from Sigma-Aldrich and used at a concentration of 10 µM. Cell were treated with nocodazole for 2 h prior to fixation.

Lentiviral infection and cell line selection

Lentivirus packaging was performed by using MaxPEI-based co-transfection of HEK293T cells with psPAX2, pMD2.G and the lentiviral vector pSIN-TRE-rtTA-IRES-Hygro-iLID-dTomato-RAB11A. Supernatant of packaging cells was harvested up to 72 h of transfection, filtered through a 0.45-µm filter and incubated with a polyethylene glycol (PEG)-6000-based precipitation solution overnight at 4°C. After precipitation, virus was concentrated up to 100× by centrifugation and dissolution in 1× phosphate buffered saline (PBS). Target cells were incubated for 4 h in complete medium supplemented with 8 µg/ml polybrene before infection. To establish clonal Caco-2 stable lines carrying doxycycline-inducible dTomato–Rab11A, medium was replaced 24–48 h after infection and 100 µg/ml hygromycin (Invitrogen) was added.

Immunofluorescence staining of fixed samples

For immunofluorescent staining of 2D cultures, cells were fixed with either 4% PFA for 20 min at room temperature (ezrin, CEP135, phosphorylated ERM, phalloidin) or −20°C MeOH for 10 min (α-tubulin, CAMSAP2, aPKC, ZO-1, ACF7, CAMSAP3, actin, E-cadherin, γ-tubulin) followed by permeabilization with 0.2% Triton X-100 for 2 min. Next, samples were blocked with 1% BSA diluted in 1× PBS supplemented with 0.05% Tween-20 for 45 min and sequentially incubated with primary antibodies for 1 h and fluorescently labeled secondary antibodies for 45 min. Finally, samples were washed, dried and mounted in DAPI-containing Vectashield (Vector laboratories).

For immunofluorescence staining of 3D cultures, cells were fixed with 4% PFA for 20 min at room temperature, rinsed with 1× PBS with glycine (10× stock: 38.00 g NaCl, 9.38 g Na_2HPO_4, 2.07 g NaH_2PO_4, 37.50 g glycine in 500 ml milliQ water, pH 7.4) followed by permeabilization

with 0.5% Triton X-100 in 1× PBS with glycine for 20 min. Next, samples were blocked with 1% BSA diluted in 1× immunofluorescence wash buffer (10× stock: 38.00 g NaCl, 9.38 g Na_2HPO_4, 2.07 g NaH_2PO_4, 2.5 g NaN_2, 10 ml Triton X-100, 2.5 ml Tween-20 in 500 ml milliQ water, pH 7.4) for 45 min and sequentially incubated with primary antibodies for 2 h at 37°C and fluorescently labeled secondary antibodies for 1.5 h at room temperature. Finally, samples were washed and mounted in DAPI-containing Vectashield.

Microscopy and image analysis

2D confluent monolayers and 3D cultures were imaged by using confocal fluorescence illumination on a Nikon Eclipse Ti microscope equipped with a perfect focus system (PFS, Nikon), a spinning-disc-based confocal scanner unit (CSU-X1-A1, Yokogawa), an Evolve 512 EMCCD camera (Photometrics) attached to a 2.0× intermediate lens (Edmund Optics), a super-high-pressure mercury lamp (C-SHG1, Nikon), a Roper Scientific custom-made set of Stradus 405-nm (100 mW, Vortran), Calypso 491-nm (100 mW, Cobolt) and Jive 561-nm (100 mW, Cobolt) lasers, a set of ET-BFP2, ET-EGFP, ET-mCherry and ET-EGFP-mCherry filters (Chroma) for wide-field fluorescence observation, a set of ET460/50m, ET525/50m or ET535/30m (green), ET630/75m (red) and ET-EGFP/mCherry filters (Chroma) for spinning-disc-based confocal imaging and a motorized stage MS-2000-XYZ with Piezo Top Plate (ASI). The microscope setup was controlled by MetaMorph 7.7.11.0 software. Images were acquired using Plan Fluor 10× NA 0.3 air, Plan Fluor 20× MI NA 0.75 oil, Plan Apochromat λ 60× NA 1.4 oil and Plan Apo VC 60× NA 1.4 oil objectives. This system was also used for FRAP experiments using the iLas2 system (Roper Scientific).

z-series images of 2D confluent layers were acquired using a 0.1-µm-step confocal-based scan. Side views were reconstructed by projecting maximum fluorescence intensities of 50×0.11-µm side view slices. The apical–basal polarity index was determined by using side views as described above in the following equation: $\frac{Fa}{Fb} - 1$, in which F_a is the fluorescent intensity in the upper one-third of the side view corrected for the area and F_b is the fluorescence intensity in the lower two-thirds of the side view corrected for the area. For presentation, images were adjusted for brightness using ImageJ 1.50b. FRAP measurements were performed by bleaching a 8.8-µm-diameter circle in the apical side of a cell monolayer followed by 15 min of imaging with a frame interval of 10 s.

Phase contrast images were acquired on a Nikon Ti instrument equipped with a perfect focus system (PFS, Nikon), a super-high-pressure mercury lamp (C-SHG1, Nikon), Lambda SC Smart Shutter controllers (Sutter), a Plan Apochromat DM 20× NA 0.75 (Ph2) or a Plan Fluor DLL 10× NA 0.3 (Ph1), an ET-mCherry filter (Chroma), a CoolSNAP HQ^2 CCD camera (Photometrics), a motorized stage MS-2000-XYZ with Piezo Top Plate (ASI) and a stage top incubator INUG2E-ZILCSD-DV (Tokai Hit) for 37°C under 5% CO_2. The microscope setup was controlled by the open source microscopy software Micro-manager.

To determine protein knockdown efficiency by immunofluorescence staining, cells were imaged on a Nikon Eclipse 80i upright microscope equipped with a CoolSNAP HQ^2 CCD camera (Photometrics), an Intensilight C-HGFI precentered fiber illuminator (Nikon), ET-DAPI, ET-EGFP and ET-mCherry filters (Chroma), controlled by Nikon NIS Br software and using a Plan Apo VC 100× NA 1.4 oil, Plan Apo VC 60× NA 1.4 oil or a Plan Fluor 20× MI NA 0.75 oil objective (Nikon). For knockdown efficiency tests, fluorescence intensity was measured per cell and corrected for the cell surface area using ImageJ 1.50b.

Microtubule organization in CAMSAP-knockout lines was imaged by confocal fluorescence illumination on a Leica TCS SP8 STED3X SMD FLIM Super Resolution instrument and confocal microscope equipped with adaptive focus control, a filter-free Spectral Leica SP detector and HyD detector, a 405-nm DMOD and a fully tunable supercontinuum white laser (470 to 670 nm). Images were acquired using a HC PL APO Cs2 100×1.40 oil objective. *z*-series were acquired using 0.16-µm- (Control) and 0.22-µm- (CAMSAP2 and CAMSAP3 knockout) step confocal-based scan. Images are presented as maximum projections and were adjusted for brightness using ImageJ 1.50b.

RT-PCR and quantitative PCR analysis

Total RNA was extracted from Caco-2 cells using Trizol reagent (Thermo Fisher Scientific) and used as a template for reverse transcription (RT-PCR) with random hexamer primers (Thermo Fisher Scientific). After DNase treatment (Thermo Fisher Scientific), cDNA was submitted to quantitative real-time (q)PCR using Sybrgreen technology (Applied Biosystems) on a ViiA7 apparatus (Applied Biosystems). Two *ACF7* and two reference gene (*HPRT1* and *GAPDH*) primer pairs were used to quantify *ACF7* relative expression following siRNA transfection using the ΔΔCt method. Primer sequences were as followed: ACF7 #1, 5′- GGTCCTCTCAGGCATCAA-AC-3′, 5′-AGTTTCACCTGTCGCTGCTT-3′; ACF7 #2, 5′-TGCACTCA-TTCACCGATACC-3′, 5′-CCCAGTCTTTCTGCCACTTC-3′; HPRT1, 5′-TGCAGACTTTGCTTTCCTTGGTCAGG-3′, 5′-CCAACACTTCGTGG-GGTCCTTTTCA-3′; GAPDH, 5′-CTTCGCTCTCTGCTCCTCCTGTTC-G-3′, 5′-ACCAGGCGCCCAATACGACCAAAT-3′.

Statistical analysis

All experiments were conducted at least twice. Statistical analysis was performed using GraphPad Prism 5.

Acknowledgements

We thank J. L. Bos (UMC Utrecht, The Netherlands), A. Yap (University of Queensland, Australia), B. Bouchet (Utrecht University, The Netherlands), R. Pagano (Mayo Clinic College of Medicine, Rochester, MN), B. Kuhlman (University of North Carolina, Chapel Hill, NC) for the gifts of materials, and J. Demmers (Erasmus MC, Rotterdam, The Netherlands) for performing mass spectrometry analysis.

Competing interests

The authors declare no competing or financial interests.

Author contributions

I.N., L.C.K. and A.A. designed experiments and wrote the paper. A.A. coordinated the project. I.N., Q.L., M.B., S.R. and M.M. generated tools and performed the experiments, W.N., S.H. and K.J. generated tools.

Funding

This study was supported by the Netherlands Organization for Scientific Research (Nederlandse Organisatie voor Wetenschappelijk Onderzoek) ALW Open program (grant 822.02.002) and the CW ECHO (grant 711.015.005).

Supplementary information

Supplementary information available online at
http://jcs.biologists.org/lookup/doi/10.1242/jcs.194878.supplemental

References

Akhmanova, A. and Hoogenraad, C. C. (2015). Microtubule minus-end-targeting proteins. *Curr. Biol.* **25**, R162-R171.

Baas, A. F., Kuipers, J., van der Wel, N. N., Batlle, E., Koerten, H. K., Peters, P. J. and Clevers, H. C. (2004). Complete polarization of single intestinal epithelial cells upon activation of LKB1 by STRAD. *Cell* **116**, 457-466.

Baines, A. J., Bignone, P. A., King, M. D. A., Maggs, A. M., Bennett, P. M., Pinder, J. C. and Phillips, G. W. (2009). The CKK domain (DUF1781) binds microtubules and defines the CAMSAP/ssp4 family of animal proteins. *Mol. Biol. Evol.* **26**, 2005-2014.

Bartolini, F. and Gundersen, G. G. (2006). Generation of noncentrosomal microtubule arrays. *J. Cell Sci.* **119**, 4155-4163.

Booth, A. J. R., Blanchard, G. B., Adams, R. J. and Röper, K. (2014). A dynamic microtubule cytoskeleton directs medial actomyosin function during tube formation. *Dev. Cell* **29**, 562-576.

Bornens, M. (2012). The centrosome in cells and organisms. *Science* **335**, 422-426.

Bryant, D. M., Datta, A., Rodriguez-Fraticelli, A. E., Peranen, J., Martin-Belmonte, F. and Mostov, K. E. (2010). A molecular network for de novo generation of the apical surface and lumen. *Nat. Cell Biol.* **12**, 1035-1045.

Dambournet, D., Machicoane, M., Chesneau, L., Sachse, M., Rocancourt, M., El Marjou, A., Formstecher, E., Salomon, R., Goud, B. and Echard, A. (2011). Rab35 GTPase and OCRL phosphatase remodel lipids and F-actin for successful cytokinesis. *Nat. Cell Biol.* **13**, 981-988.

Dammermann, A., Desai, A. and Oegema, K. (2003). The minus end in sight. *Curr. Biol.* **13**, R614-R624.

Dhekne, H. S., Hsiao, N.-H., Roelofs, P., Kumari, M., Slim, C. L., Rings, E. H. H. M. and van Ijzendoorn, S. C. D. (2014). Myosin Vb and Rab11a regulate phosphorylation of ezrin in enterocytes. *J. Cell Sci.* **127**, 1007-1017.

Drabek, K., van Ham, M., Stepanova, T., Draegestein, K., van Horssen, R., Sayas, C. L., Akhmanova, A., Ten Hagen, T., Smits, R., Fodde, R. et al. (2006). Role of CLASP2 in microtubule stabilization and the regulation of persistent motility. *Curr. Biol.* **16**, 2259-2264.

Goodwin, S. S. and Vale, R. D. (2010). Patronin regulates the microtubule network by protecting microtubule minus ends. *Cell* **143**, 263-274.

Hendershott, M. C. and Vale, R. D. (2014). Regulation of microtubule minus-end dynamics by CAMSAPs and Patronin. *Proc. Natl. Acad. Sci. USA* **111**, 5860-5865.

Horgan, C. P., Hanscom, S. R., Jolly, R. S., Futter, C. E. and McCaffrey, M. W. (2010). Rab11-FIP3 links the Rab11 GTPase and cytoplasmic dynein to mediate transport to the endosomal-recycling compartment. *J. Cell Sci.* **123**, 181-191.

Jaffe, A. B., Kaji, N., Durgan, J. and Hall, A. (2008). Cdc42 controls spindle orientation to position the apical surface during epithelial morphogenesis. *J. Cell Biol.* **183**, 625-633.

Jiang, K., Hua, S., Mohan, R., Grigoriev, I., Yau, K. W., Liu, Q., Katrukha, E. A., Altelaar, A. F. M., Heck, A. J. R., Hoogenraad, C. C. et al. (2014). Microtubule minus-end stabilization by polymerization-driven CAMSAP deposition. *Dev. Cell* **28**, 295-309.

Karakesisoglou, I., Yang, Y. and Fuchs, E. (2000). An epidermal plakin that integrates actin and microtubule networks at cellular junctions. *J. Cell Biol.* **149**, 195-208.

Khanal, I., Elbediwy, A., Diaz de la Loza, M. C., Fletcher, G. C. and Thompson, B. J. (2016). Shot and Patronin polarise microtubules to direct membrane traffic and biogenesis of microvilli in epithelia. *J. Cell Sci.* **129**, 2651-2659.

King, M. D. A., Phillips, G. W., Bignone, P. A., Hayes, N. V. L., Pinder, J. C. and Baines, A. J. (2014). A conserved sequence in calmodulin regulated spectrin-associated protein 1 links its interaction with spectrin and calmodulin to neurite outgrowth. *J. Neurochem.* **128**, 391-402.

Knowles, B. C., Weis, V. G., Yu, S., Roland, J. T., Williams, J. A., Alvarado, G. S., Lapierre, L. A., Shub, M. D., Gao, N. and Goldenring, J. R. (2015). Rab11a regulates syntaxin 3 localization and microvillus assembly in enterocytes. *J. Cell Sci.* **128**, 1617-1626.

Kodama, A., Karakesisoglou, I., Wong, E., Vaezi, A. and Fuchs, E. (2003). ACF7: an essential integrator of microtubule dynamics. *Cell* **115**, 343-354.

Letunic, I., Doerks, T. and Bork, P. (2015). SMART: recent updates, new developments and status in 2015. *Nucleic Acids Res.* **43**, D257-D260.

Meng, W., Mushika, Y., Ichii, T. and Takeichi, M. (2008). Anchorage of microtubule minus ends to adherens junctions regulates epithelial cell-cell contacts. *Cell* **135**, 948-959.

Moss, D. K., Bellett, G., Carter, J. M., Liovic, M., Keynton, J., Prescott, A. R., Lane, E. B. and Mogensen, M. M. (2007). Ninein is released from the centrosome and moves bi-directionally along microtubules. *J. Cell Sci.* **120**, 3064-3074.

Nashchekin, D., Fernandes, A. R. and St Johnston, D. (2016). Patronin/shot cortical foci assemble the noncentrosomal microtubule array that specifies the Drosophila anterior-posterior axis. *Dev. Cell* **38**, 61-72.

Overeem, A. W., Bryant, D. M. and van IJzendoorn, S. C. D. (2015). Mechanisms of apical-basal axis orientation and epithelial lumen positioning. *Trends Cell Biol.* **25**, 476-485.

Ran, F. A., Hsu, P. D., Wright, J., Agarwala, V., Scott, D. A. and Zhang, F. (2013). Genome engineering using the CRISPR-Cas9 system. *Nat. Protoc.* **8**, 2281-2308.

Ratheesh, A., Gomez, G. A., Priya, R., Verma, S., Kovacs, E. M., Jiang, K., Brown, N. H., Akhmanova, A., Stehbens, S. J. and Yap, A. S. (2012). Centralspindlin and alpha-catenin regulate Rho signalling at the epithelial zonula adherens. *Nat. Cell Biol.* **14**, 818-828.

Riggs, B., Fasulo, B., Royou, A., Mische, S., Cao, J., Hays, T. S. and Sullivan, W. (2007). The concentration of Nuf, a Rab11 effector, at the microtubule-organizing center is cell cycle regulated, dynein-dependent, and coincides with furrow formation. *Mol. Biol. Cell* **18**, 3313-3322.

Schultz, J., Milpetz, F., Bork, P. and Ponting, C. P. (1998). SMART, a simple modular architecture research tool: identification of signaling domains. *Proc. Natl. Acad. Sci. USA* **95**, 5857-5864.

Sobajima, T., Yoshimura, S.-I., Iwano, T., Kunii, M., Watanabe, M., Atik, N., Mushiake, S., Morii, E., Koyama, Y., Miyoshi, E. et al. (2015). Rab11a is required for apical protein localisation in the intestine. *Biol. Open* **4**, 86-94.

Takahashi, S., Mui, V. J., Rosenberg, S. K., Homma, K., Cheatham, M. A. and Zheng, J. (2016). Cadherin 23-C regulates microtubule networks by modifying CAMSAP3's function. *Sci. Rep.* **6**, 28706.

Tanaka, N., Meng, W., Nagae, S. and Takeichi, M. (2012). Nezha/CAMSAP3 and CAMSAP2 cooperate in epithelial-specific organization of noncentrosomal microtubules. *Proc. Natl. Acad. Sci. USA* **109**, 20029-20034.

Toya, M., Kobayashi, S., Kawasaki, M., Shioi, G., Kaneko, M., Ishiuchi, T., Misaki, K., Meng, W. and Takeichi, M. (2016). CAMSAP3 orients the apical-to-basal polarity of microtubule arrays in epithelial cells. *Proc. Natl. Acad. Sci. USA* **113**, 332-337.

Viswanatha, R., Ohouo, P. Y., Smolka, M. B. and Bretscher, A. (2012). Local phosphocycling mediated by LOK/SLK restricts ezrin function to the apical aspect of epithelial cells. *J. Cell Biol.* **199**, 969-984.

Wang, S., Wu, D., Quintin, S., Green, R. A., Cheerambathur, D. K., Ochoa, S. D., Desai, A. and Oegema, K. (2015). NOCA-1 functions with gamma-tubulin and in parallel to Patronin to assemble non-centrosomal microtubule arrays in C. elegans. *Elife* **4**, e08649.

Wu, X., Kodama, A. and Fuchs, E. (2008). ACF7 regulates cytoskeletal-focal adhesion dynamics and migration and has ATPase activity. *Cell* **135**, 137-148.

Wu, J., de Heus, C., Liu, Q., Bouchet, B. P., Noordstra, I., Jiang, K., Hua, S., Martin, M., Yang, C., Grigoriev, I. et al. (2016). Molecular pathway of microtubule organization at the Golgi apparatus. *Dev. Cell* **39**, 44-60.

Zheng, J., Furness, D., Duan, C., Miller, K. K., Edge, R. M., Chen, J., Homma, K., Hackney, C. M., Dallos, P. and Cheatham, M. A. (2013). Marshalin, a microtubule minus-end binding protein, regulates cytoskeletal structure in the organ of Corti. *Biol. Open* **2**, 1192-1202.

Supplemental Information

Control of apico-basal epithelial polarity by the microtubule minus-end binding protein CAMSAP3 and spectraplakin ACF7

Ivar Noordstra, Qingyang Liu, Wilco Nijenhuis, Shasha Hua, Kai Jiang, Matthijs Baars, Sanne Remmelzwaal, Maud Martin, Lukas C. Kapitein and Anna Akhmanova.

Figure s1

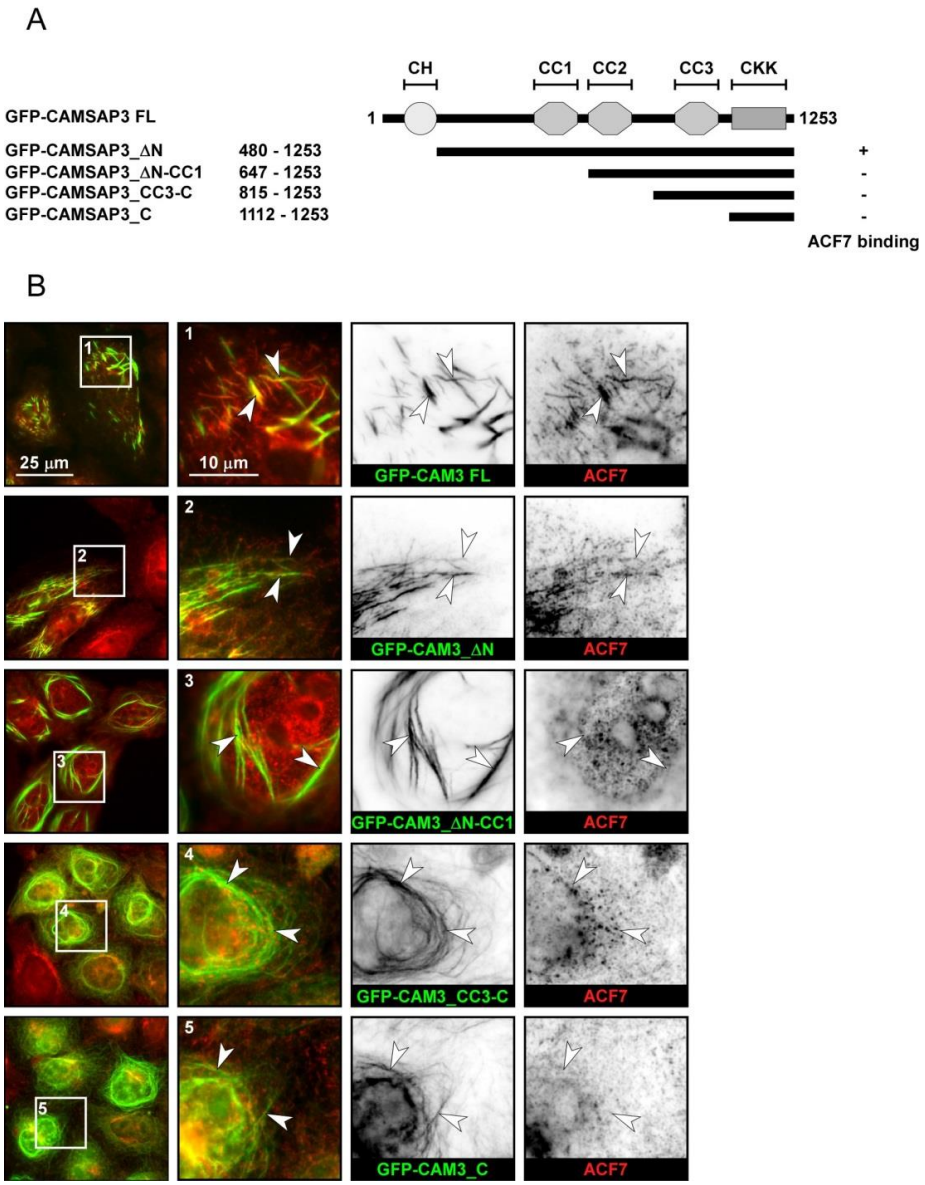

Supplemental Figure S1. Endogenous ACF7 is recruited to CAMSAP3-induced microtubule bundles in manner dependent on the CC1 region of CAMSAP3.

A. Domain organization of GFP-CAMSAP3 deletion mutants used to study binding to ACF7 and a summary of detected interactions. FL, full length, CH, calponin homology domain.

B. HeLa cells transiently expressing GFP-CAMSAP3 fragments (as in A, green) and stained for ACF7 (red). White arrowheads indicate the same positions in different panels.

Figure s2

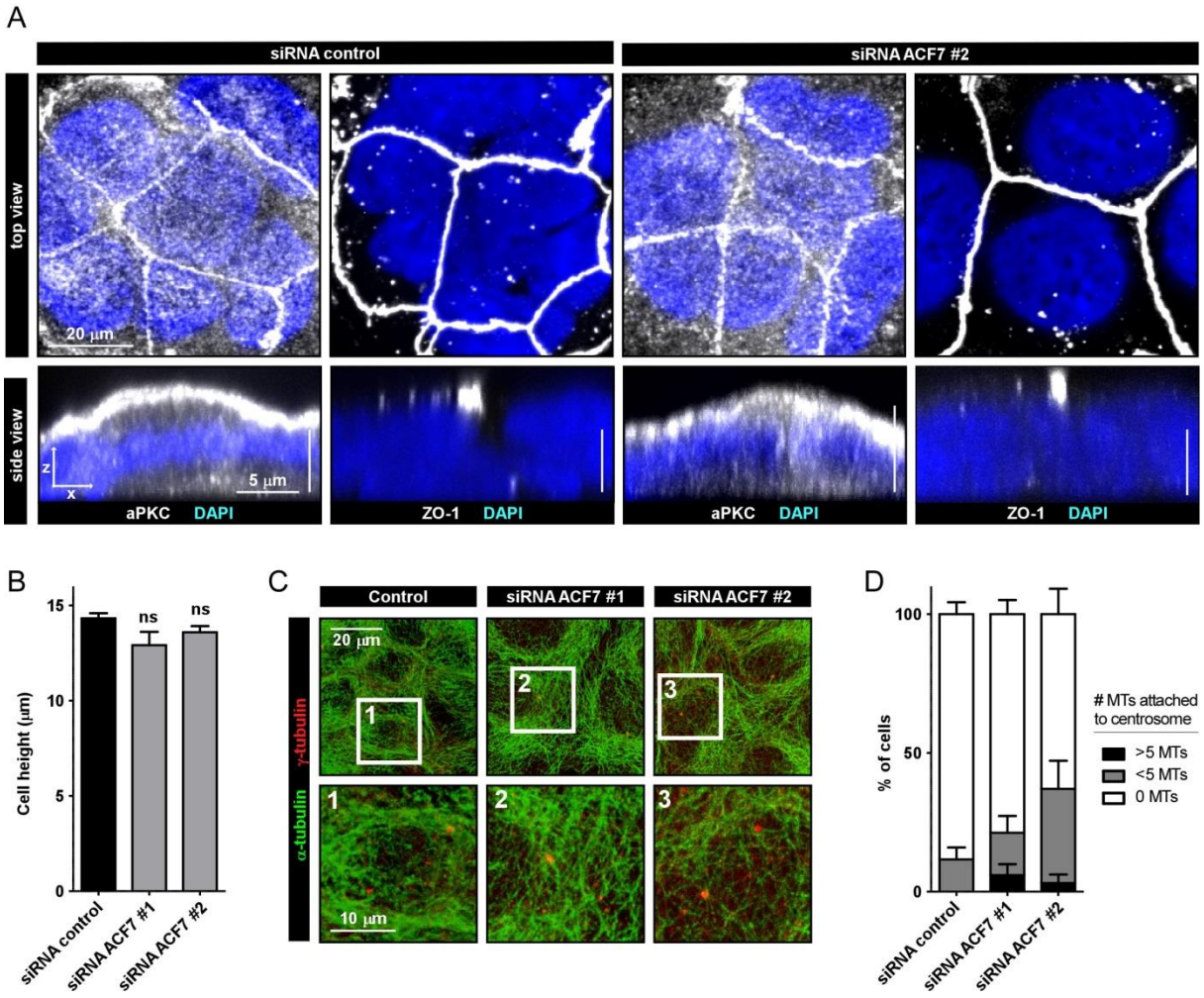

Supplemental Figure S2. ACF7 depletion does not affect general polarity in 2D monolayer culture.

A. Staining of aPKC, ZO-1 (white) and DNA (blue) in Caco-2 cells transfected with control or ACF7 siRNAs. Both top and side views are shown.

B. Quantification of cell height of Caco-2 cells transfected with control or ACF7 siRNAs. Control, n=36; siRNA ACF7 #1, n=36; siRNA ACF7 #2, n=36; ns, not significant; Mann-Whitney U test; Error bars, SEM.

C. Staining of microtubules (green, α-tubulin) and centrosomes (red, ɣ-tubulin) in Caco-2 cells transfected with control or ACF7 siRNAs.

D. Quantification of microtubule organization presented as a number of microtubules attached to the centrosome. Quantification based on staining shown in (C). Number of analyzed cells: control, n=41; siRNA ACF7 #1, n=38; siRNA ACF7 #2, n=60; Error bars, SEM; #, number; MTs, microtubules.

Figure s3

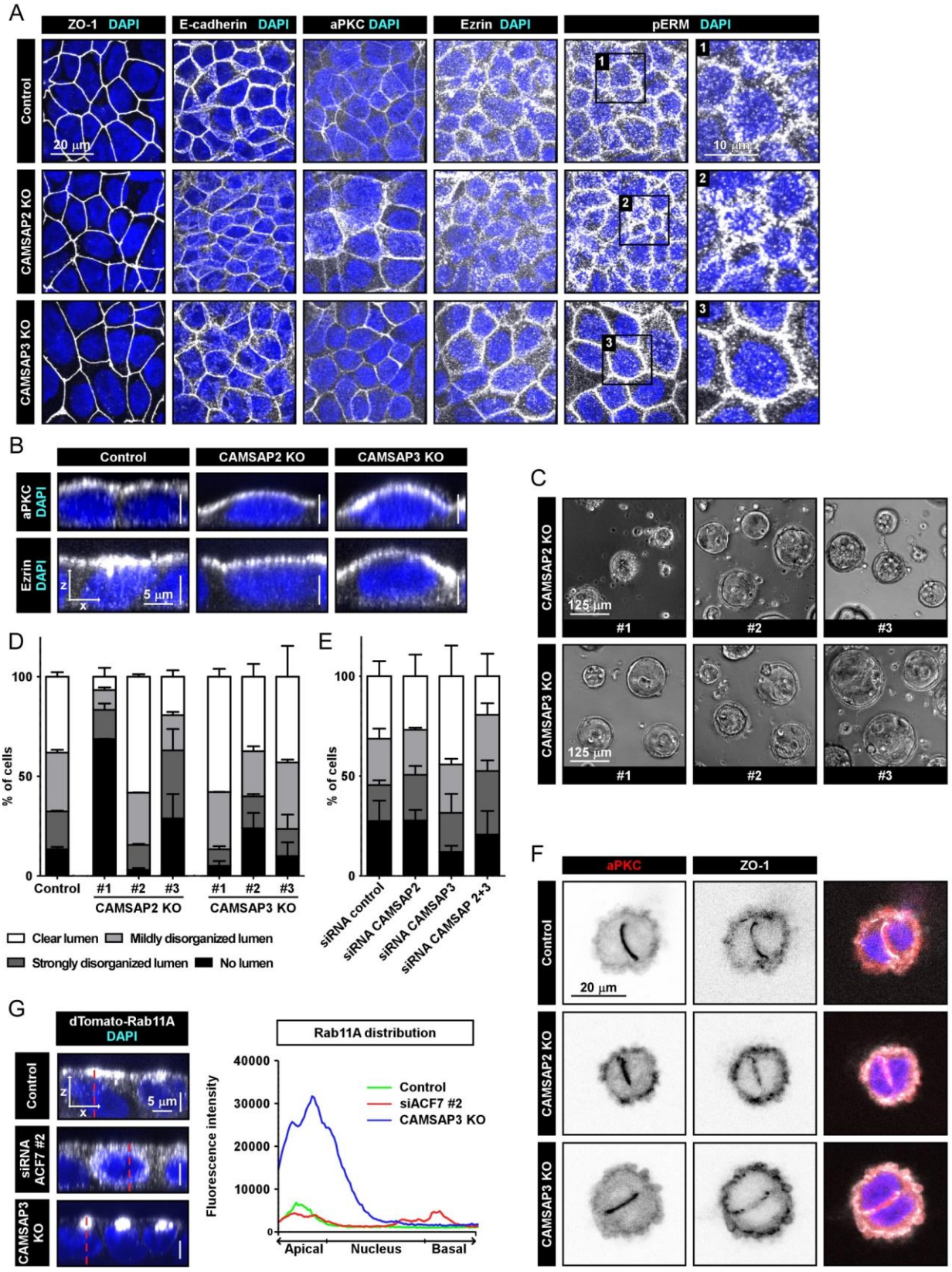

Supplemental Figure S3. Formation of 3D cysts and the distribution of polarity markers in control, CAMSAP2 and CAMSAP3 knockout cells.

A. Staining for ZO-1, E-cadherin, aPKC, ezrin en pERM (white) and DNA (blue) in control, CAMSAP2 and CAMSAP2 knockout (KO) cells.

B. Side view of aPKC, ezrin (white) and DNA (blue) staining in cells as in (A).

C. 3D cyst formation 1 day after dense seeding of different CAMSAP2 and CAMSAP3 knockout clones.

D. Quantification of 3D cyst formation of cells in (C). Control, n=200; CAMSAP2 KO #1, n=172; CAMSAP2 KO #2, n=245; CAMSAP2 KO #3, n=143; CAMSAP3 KO #1, n=173; CAMSAP3 KO #2, n=204; CAMSAP3 KO #3, n=213.

E. Quantification of 3D cyst formation of Caco-2 cells transfected with siRNA targeting CAMSAP2, CAMSAP3 or CAMSAP2 and 3 simultaneously. siRNA control, n=320; siRNA CAMSAP2, n=226; siRNA CAMSAP3, n=316; siRNA CAMSAP2+3, n=252.

F. Staining of aPKC (red), ZO-1 (white) and DNA (blue) in cells as in (A) seeded in a 3D matrix.

G. Side view of dTomato-Rab11A (white) and DNA (blue) in control cells, cells transfected with siRNA targeting ACF7 and CAMSAP3 knockout cells. dTomato-Rab11A intensity profiles along the line indicated in red are plotted in the graph.

Supplemental table 1

Primary antibodies

Target	Source	Dilution	Company	Catalog number
Tyrosinated α-tubulin	Rat	IF 1:300	Abcam	#ab6160
mCherry	Mouse	WB 1:1000	Clontech	#632543
ACF7	Mouse	IF 1:400	Abnova	#H00023499-A01
CAMSAP3	Mouse	IF 1:200 WB 1:1000	Sigma-Aldrich	#SAB4200415
ɣ-tubulin	Mouse	IF 1:100	Sigma-Aldrich	#T5326
Ku80	Mouse	WB 1:2000	BD Biosciences	#611360
ZO-1	Mouse	IF 1:500	BD Biosciences	#610966
E-cadherin	Mouse	IF 1:500	BD Biosciences	#610181
Ezrin	Mouse	IF 1:500	BD Biosciences	#610602
GFP	Rabbit	WB 1:1000	Abcam	#ab290
CAMSAP2	Rabbit	IF 1:300	Novus	#NBP1-21402
CAMSAP2	Rabbit	WB 1:1000	Proteintech	#17880-1-AP
aPKC	Rabbit	IF 1:300	Santa Cruz	#H00023499-A01
Actin	Rabbit	IF 1:200	Sigma-Aldrich	#20-33
CEP135	Rabbit	IF 1:300	Sigma-Aldrich	#SAB4503685
Phosphorylated ERM	Rabbit	IF 1:500	Cell Signaling	#3141
E-cadherin	Rabbit	IF 1:1000	Gift from A. Yap	-

IF: Immunofluorescence staining
WB: Western blot

Secondary antibodies

All secondary antibodies used for immunofluorescence staining were diluted 1:300
All secondary antibodies used for western blot were diluted 1:15000